Check for updates

Electric field analyses on monolayer semiconductors: the example of InSe†

Xue-Peng Wang,[a] Xian-Bin Li, ⓘD*[a] Nian-Ke Chen,[a] Ji-Hong Zhao,[a] Qi-Dai Chen[a] and Hong-Bo Sun ⓘD [ab]

External electric fields can be used to manipulate the electronic properties of two-dimensional (2D) materials. 2D InSe semiconductors possess high electron mobility and wide band gap tunability. Therefore, they have been proposed for use in ultrathin electronic devices. Here, using first-principles calculations, we study the charge polarization, structure, electronic structure, and gas adsorption of an InSe monolayer under vertical electric fields. We find that both the structural evolution and charge polarization rely on the directions of the electric fields. The hole effective mass at the valance band maximum can be decreased by fields that offer a possible route to increase mobility. In contrast, the fields have little impact on the effective mass of electrons at the conduction band minimum. Therefore, high electron mobility in InSe is retained under the fields. Besides, electric fields could alter the absorption intensity for gas molecules. Therefore, gas sensors could be an expected application. More importantly, this work systematically points out some key steps for setting up electric-field calculations in the popular VASP code, such as the cancellation of the symmetrisation of the charge density, avoiding electrons spilling out into the vacuum under high fields.

Introduction

Ultrathin two-dimensional (2D) semiconductors may have high carrier mobilities.[1–3] These materials have shown prospects for use in flexible optoelectronics.[4,5] Because of the gapless nature of graphene,[6,7] a series of layered transition metal chalcogenides with well-defined bandgaps, such as MoS_2,[8–10] WSe_2,[11] and InSe, have been proposed. Most recently, 2D InSe has drawn considerable attention due to it having the possible highest electron mobility reported for 2D chalcogenides ($\sim$1000 cm^2 V^{-1} s^{-1} for 6-layer InSe at room temperature).[12] Many efforts have been made to study its defects,[13,14] phase transition,[15] spectrum,[16] and surface functionalization.[17] Field effect transistors (FET) with 2D InSe as transport channels have been reported.[12,18] Photodetectors based on few-layered InSe also show broad spectral responses.[19,20] In addition, 2D InSe is considered as a promising candidate for gas sensors.[21,22] An InSe monolayer has a honeycomb lattice, as shown in Fig. 1(a). The central pairs of In atoms form homogeneous bonds, and each of them connects with three other Se atoms in the outer layer. Bulk InSe has a direct band gap.[23] Its band gap
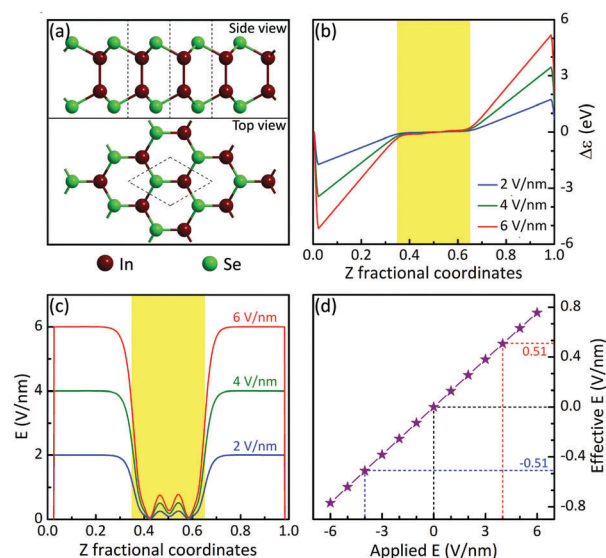

Fig. 1 (a) A schematic diagram of an InSe monolayer. Color coding: dark brown for In; and green for Se. (b) Potential energy differences ($\Delta\varepsilon$) induced by electric fields along the Z direction. (c) Electric field intensity distribution along the Z direction (vertical to the plane). The region shaded in yellow indicates the thickness of the InSe monolayer. (d) The effective electric field intensity (effective E) in the InSe region as a function of the applied value (applied E).

increases sharply as the number of layers decreases.[24–26] When the thickness goes down to about ten layers, InSe exhibits an indirect gap.[24]

[a] State Key Laboratory of Integrated Optoelectronics, College of Electronic Science and Engineering, Jilin University, Changchun, 130012, China

[b] State Key Lab of Precision Measurement Technology and Instruments, Department of Precision Instrument, Tsinghua University, Beijing, 100084, China. E-mail: lixianbin@jlu.edu.cn

† Electronic supplementary information (ESI) available. See DOI: 10.1039/c7cp07270h

This journal is © the Owner Societies 2018

Phys. Chem. Chem. Phys., 2018, **20**, 6945–6950 | 6945

Generally, 2D materials are sensitive to external conditions.[27] In other words, external conditions or methods can be used to control their properties. Using an external electric field is one such method that is usually used in electronic devices. Electric fields can easily affect structures, charge distributions, and conductive channels in 2D materials. For example, density functional theory (DFT) calculations have suggested that electric fields could be used to tailor the band gaps in GaN monolayers (modified with H and F),[28] blue phosphorus,[29] rippled MoS_2 monolayers,[30] and also bilayer MoS_2, $MoSe_2$, $MoTe_2$, and WS_2.[31] Furthermore, electric fields can also enhance the adsorption of H_2 on 2D BN.[32] As such, this is a possible way to increase the sensitivity of 2D gas sensors using electric fields. However, there is still some confusion about the electric-field effect on 2D materials in calculations. For example, an electric field induces layer-to-layer charge transfer in MoS_2/WS_2 and MoS_2/black phosphorus van der Waals heterostructures.[33,34] In contrast, in bilayer MoS_2, charge accumulation happens in the region between the two layers (inside the van der Waals gap) under electric fields.[31] Besides, it is proposed that electric fields cannot easily change the band gap of a MoS_2 monolayer.[31] However, a semiconductor-to-metal transition in a InSe monolayer under electric fields has been predicted.[35] Therefore, there are still a lot of questions to answer regarding the effects of electric fields on 2D materials.

In this work, we take an InSe monolayer as an example to study the effects of vertical electric fields on the charge polarization, structure, electronic structure, and gas molecule adsorption of 2D materials, using first-principles calculations. We find that electric fields mainly induce charge polarization in the Se layers. Under a vertical electric field, the upper and lower surfaces of InSe show opposite charge characteristics, manifesting as electronic polarization. The In–Se bond length depends on the intensity and direction of the electric fields. However, the field has little impact on In–In bonds. Regarding the electronic structure, the effective mass of holes at the valence band maximum is easier to change (decrease) using electric fields in contrast to that of electrons at the conduction band minimum. Finally, we study gas adsorption (H_2) on both surfaces of an InSe monolayer under electric fields. The binding abilities of molecules on the two surfaces show differences, and can be manipulated using the fields. Our study indicates that electric fields are a tool to control the electronic properties of InSe for potential devices, such as gas sensors.

Methods

Our DFT calculations are performed with projected augmented wave (PAW) formalism,[36,37] as implemented in VASP codes.[38] The electron exchange–correlation interaction is described using the Perdew–Burke–Ernzerhof (PBE) functional.[39] We use 325 eV as the cutoff energy for the plane wave basis set and $8 \times 8 \times 1$ Monkhorst–Pack k-points. Spin polarization has been considered in the calculations and an InSe monolayer exhibits non-magnetic features. In our model, a 20 Å vacuum layer is used. The external electric field is perpendicular to the plane of the InSe monolayer (along the Z direction of the cell). To get the correct results, it should be stressed that the default symmetrisation of the charge density must be cancelled in calculations when an electric field is applied. Otherwise, the charge polarization behavior would encounter serious problems in the VASP code; see details in Part 1 of the (ESI†) for more information. For the H_2 adsorption model, we use a $3 \times 3 \times 1$ InSe supercell which contains 18 In atoms, 18 Se atoms, and 2 H_2 molecules. The van der Waals interactions are corrected using the Grimme DFT-D2 method.[40] The binding energy of H_2 on one side is referred to the energy of InSe plus H_2 on the other side.

Results and discussion

Due to screening effects in the material, the effective electric field on InSe is not the applied value and thus should be calibrated. For this purpose, we study electrostatic potential energy distributions in the calculations. To exclude the impacts of structural change, all atoms are fixed. Since the electric field is along the Z direction, we only calculate the average electronic electrostatic potential energy along the Z direction, as shown in Fig. 2(a)–(c). Then, we get the potential energy differences ($\Delta\varepsilon = \varepsilon_E - \varepsilon_0$) caused by the electric fields, as shown in Fig. 1(b). Here, ε_E and ε_0 stand for the electrostatic potential energies under E V nm^{-1} and 0 V nm^{-1} electric fields, respectively. Accordingly, we can obtain the intensity of the external electric field along the Z direction using

$$E = \frac{\mathrm{d}\varphi}{\mathrm{d}z} = \frac{\mathrm{d}\Delta\varepsilon}{-e\mathrm{d}z}$$

where φ is the electronic electrostatic potential, z is the distance along the Z direction, and e is the elementary charge. By differentiating the potential energy difference, the distribution of the electric field intensity can be obtained, as shown in Fig. 1(c). Here, the Z fractional coordinates from 0.35 to 0.65 correspond to the region of the InSe monolayer, highlighted by the yellow color. When the applied electric field is up to 6 V nm^{-1}, the intensity in the vacuum is exactly equal to the applied value. In contrast, the intensity in InSe is significantly small due to the screening effects of the material. Here, we take the average intensity in the InSe monolayer as the effective electric field intensity. As displayed in Fig. 1(d), the intensity of the effective field is about 1/8 of the applied value. Since the atoms are fixed, the reduction in the applied field is due to electronic screening. In fact, the reduction in the external field in the InSe monolayer also matches the difference in the dielectric constants between the vacuum and the material; see details in Part 2 of the ESI† for more information. As a result, most of the potential energy drop occurs in the vacuum and a small effective field exists in the material. This will be true in experimental devices, but the field would not be over a vacuum but over a high-k dielectric in a transistor structure.

It has been predicted that an InSe monolayer will transform to a metallic state under a 10 V nm^{-1} high field.[35] Here, we also

6946 | *Phys. Chem. Chem. Phys.*, 2018, **20**, 6945–6950
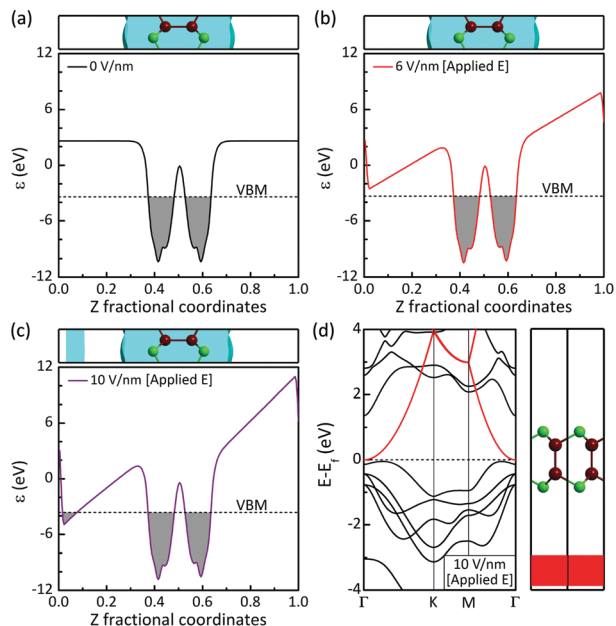
This journal is © the Owner Societies 2018

Fig. 2 Charge density and electronic potential energy distributions in an InSe monolayer under (a) 0 V nm^{-1}, (b) 6 V nm^{-1}, and (c) 10 V nm^{-1} applied electric fields along the +Z direction. The cyan isosurface corresponds to 4×10^{-5} a.u. of charge density. Regions shaded in gray are the ones filled by electrons. (d) The band structure of an InSe monolayer under a 10 V nm^{-1} applied electric field. The lowest conduction band is highlighted by the red line, and the states which contribute to this band (from the Fermi level to 1 eV above) are shown by a charge density of 1×10^{-3} a.u. (red region). The atom color coding is the same as in Fig. 1.

Fig. 3 (a) The charge density differences in the InSe monolayer under +0.25 V nm^{-1}, +0.38 V nm^{-1}, +0.51 V nm^{-1} and −0.51 V nm^{-1} effective electric fields. Yellow and cyan isosurfaces correspond to positive and negative values of 2×10^{-4} a.u., respectively. (b) The bond lengths of In−In (dark brown), upper In−Se (In−Se2, blue), and lower In−Se (In−Se1, green) versus the effective electric field. The inset shows the movement direction (red arrows) of In and Se atoms under a +Z electric field. The atom color coding is the same as in Fig. 1.

investigate how such a transition happens. As shown in Fig. 2(b) and (c), an electric field leads to a triangular potential energy distribution. Under a 6 V nm^{-1} applied field, electrons are strictly located in the InSe monolayer, while under a 10 V nm^{-1} applied field, small amounts of electrons will spill out into the vacuum, as displayed in Fig. 2(c). Meanwhile, in this case we find that the InSe monolayer has transformed to a "metallic state" according to its band structure, as shown in Fig. 2(d). The lowest conduction band (highlighted by the red color in Fig. 2(d)) has touched the Fermi level. However, projecting this conduction band from the Fermi level to 1 eV above in real space, we find that its states come from the vacuum: see the red region in Fig. 2(d). In other words, the metallic state is the result of spurious effects of spilled electrons.[41,42] Therefore, the electric field applied in calculations should be carefully checked to avoid such a situation. In the following discussion, we will use the effective field to reflect the actual case in InSe.

Next, we investigate the charge polarization and structural evolution of the InSe monolayer under electric fields. Fig. 3(a) displays the charge density difference [CDD, $\rho(E) - \rho(0)$][43] under electric fields with different intensities and directions. From the CDD distribution, we can see that the charge polarization relies on the intensity and direction of an electric field. The electrons move in the opposite direction of the electric field, which obeys basic electrostatic laws. In addition, the CDD also indicates that an electric field can induce opposite electronic behavior on the upper and lower surfaces of InSe. For
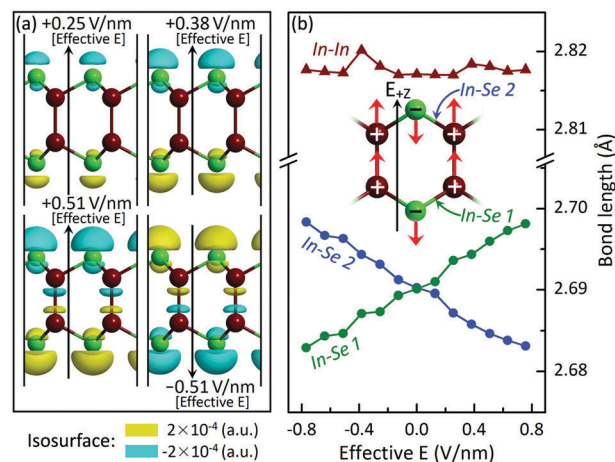
example, gas molecule adsorption can be different on the two surfaces (this will be discussed later). Under a relatively small effective electric field of 0.25 V nm^{-1}, charge polarization mainly occurs on the upper and lower surfaces around Se atoms. As the field increases, such charge polarization between Se atoms becomes more significant. Under a relatively large field, such as 0.51 V nm^{-1}, there is also charge polarization between In atoms. Furthermore, charge polarization via an electric field can also lead to small structural changes. Fig. 3(b) shows the bond length evolution for In−Se and In−In. The bond lengths of the upper (In−Se2) and lower (In−Se1) In−Se bonds exhibit opposite responses to the same electric field. For example, under a +Z field, cations (In) move upward and anions (Se) move downward; see the red arrows in the inset of Fig. 3(b) for details. Such movements will elongate In−Se1 bonds and shorten In−Se2 bonds. Since the two bonded In atoms move upward synchronously, the In−In bond length is almost unchanged. Therefore, the two bonded In atoms can be regarded as a single entity under electric fields. Here, the change in In−Se bond length is relatively small. For example, under a +0.76 V nm^{-1} effective field, the bond length of In−Se1 increases by only 0.3%.

Besides structures, electric fields can also affect band structures or their related electronic properties. Fig. 4(a)–(e) displays the band structures of an InSe monolayer under electric fields. An intrinsic InSe monolayer exhibits an indirect band gap (1.407 eV from our PBE calculations), which is consistent with previous works.[22,44] As shown in Fig. 4(a)–(e), there are no significant changes in the band structure under electric fields. This may be due to the charge polarization under the considered electric fields being relatively small. For example, according to the results of Bader analysis, only 0.029 electrons per atom have been transferred from Se in the upper layer to Se
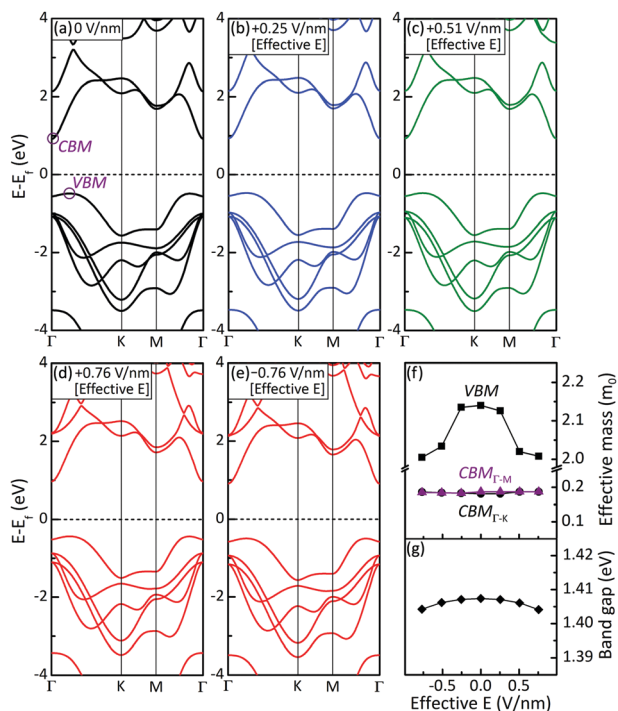
Fig. 4 The band structures of an InSe monolayer under (a) 0 V nm^{-1}, (b) +0.25 V nm^{-1}, (c) +0.51 V nm^{-1}, (d) +0.76 V nm^{-1} and (e) −0.76 V nm^{-1} effective electric fields. (f) The effective masses at the VBM (holes) and CBM (electrons, along the $\Gamma-K$ and $\Gamma-M$ directions) and (g) band gap versus the effective electric field. m_0 stands for the electron rest mass.

in the lower layer under a +0.51 V nm^{-1} effective field. However, we still find that the band gap slightly decreases as the field intensity increases: see Fig. 4(g) for details. As we know, effective mass is one of the key factors that determine the transport properties of FETs. So, it is meaningful to investigate this property. As shown in Fig. 4(f), the effective masses at the conduction band minimum (CBM, electrons) along the $\Gamma-K$ and $\Gamma-M$ directions are both quite small and very close to each other. Both of them are insensitive to the electric field, which indicates that an external field would not destroy the high mobility of electrons. The effective mass at the valance band maximum (VBM, holes) is more than 10 times larger than that of electrons at the CBM. This is consistent with it being easy for intrinsic 2D InSe to exhibit n-type conductivity.[45] Here, external electric fields can decrease the effective mass of holes at the VBM and thus enhance their mobility by a certain degree. Moreover, when an electric field is applied, the position of the VBM exhibits a weak shift toward the K-point. In contrast, the CBM remains located at the Γ-point: see details in Part 3 of the ESI† for more information. In other words, only the VBM can be modified by the fields. According to tight-binding analysis, the VBM of an InSe monolayer is mainly made up of the In s state and Se p$_Z$ state.[46] As a result, the VBM state is located between two In atoms and a spindle-shaped region along the Z direction which centers around the Se atoms (p$_Z$ orbital): see Part 4 of the ESI† for more. As mentioned above, an electric field induces charge polarization on the

upper and lower surfaces (around the Se atoms). This means that charge polarization mainly occurs in the region of the VBM state. This may be the reason why the VBM state is sensitive to external electric fields.

Finally, gas molecule adsorption on InSe under electric fields is investigated. Here, we take the simple molecule H$_2$ as an example. As mentioned above, InSe exhibits opposite charge characteristics on the upper and lower surfaces under the same electric field. So, we will investigate the H$_2$ adsorption behavior on both surfaces. In order to display polarization effects under an electric field, two H$_2$ molecules are set perpendicular to the InSe plane and reside on top of Se atoms: see Fig. 5(a) for more details. The figure also displays the CDD under a +0.51 V nm^{-1} effective field. Obviously, the electric field induces charge polarization in InSe. Such charge polarization also happens at H$_2$ and will influence the adsorption behavior on InSe. Fig. 5(b) shows the binding energy (E_b) between H$_2$ and each surface under electric fields. Without an electric field, the H$_2$ molecule on each surface has the same binding energy of 35.5 meV. As expected, the binding energies of H$_2$ on the two surfaces show different responses to the same electric field. For example, binding between H$_2$ and the lower surface of InSe is enhanced by the +Z field. In contrast, the +Z field weakens the adsorption of H$_2$ on the upper surface. The relatively small binding energy indicates that H$_2$ adsorption under an electric field still involves physisorption. H$_2$ and InSe are connected by van der Waals forces. Besides, the adsorption process is also reversible and can be controlled by the direction of the field. According to the CDD analyses in Fig. 5(a), the lower H atom of the H$_2$ molecule on the upper surface gains more electrons and becomes negatively charged under the +Z field. Meanwhile, its upper H atom becomes positively charged. For InSe, the charge density of Se atoms on the upper surface is
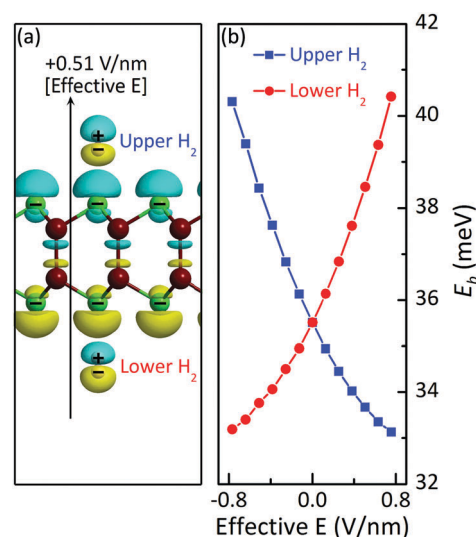

Fig. 5 (a) Charge density difference distribution in InSe with two H$_2$ molecules adsorbed, under a +0.51 V nm^{-1} effective field. Atom and CDD isosurface color coding is the same as in Fig. 3. (b) The binding energy (E_b) for the upper H$_2$ (blue line) and lower H$_2$ (red line) on InSe surfaces versus the effective field.

6948 | Phys. Chem. Chem. Phys., 2018, 20, 6945–6950

This journal is © the Owner Societies 2018

reduced by a +Z field. However, the charge density reduction is small. Through Bader analysis, we find that the electrons of a Se atom on the upper surface only decrease by 0.027e under a +0.51 V nm^{-1} field (in the presence of H$_2$). This means that Se atoms on the upper surface are still anions. As a result, they will weaken the original absorption of H$_2$ above the upper surface. Accordingly, the binding energy between H$_2$ and the lower surface of InSe will be enhanced by a +Z electric field. This indicates that selective adsorption can be achieved under electric fields in InSe.

Conclusions

In conclusion, by first-principles calculations, we investigate the effects of vertical electric fields on an InSe monolayer. Charge polarization is found to depend on the intensity and direction of the field. The electric field could slightly affect the InSe structure. Only the effective mass of holes at the VBM is sensitive to electric fields, which may offer a possible route to enhance hole mobility. Finally, we find that gas adsorption on InSe can be controlled using electric fields. This indicates that electric fields could be employed to promote adsorption or desorption in InSe-based gas sensors. Our calculations shed light on the electric field effect in 2D InSe and may offer a new pathway for its applications. Last but not least, this work also systematically points out some key steps for setting up electric-field analyses using VASP code, such as the cancellation of the symmetrisation of the charge density, avoiding electrons spilling out into the vacuum under high fields.

Conflicts of interest

There are no conflicts to declare.

Acknowledgements

References

1 Q. H. Wang, K. Kalantar-Zadeh, A. Kis, J. N. Coleman and M. S. Strano, *Nat. Nanotechnol.*, 2012, **7**, 699.

2 Y. Wu, D. Zhang, K. Lee, G. S. Duesberg, A. Syrlybekov, X. Liu, M. Abid, M. Abid, Y. Liu, L. Zhang, C. Ó. Coileáin, H. Xu, J. Cho, M. Choi, B. S. Chun, H. Wang, H. Liu and H. C. Wu, *Adv. Mater. Technol.*, 2017, **2**, 1600197.

3 X. B. Li, S. Y. Xie, H. Zheng, W. Q. Tian and H. B. Sun, *Nanoscale*, 2015, **7**, 18863.

4 F. Bonaccorso, Z. Sun, T. Hasan and A. C. Ferrari, *Nat. Photonics*, 2010, **4**, 611.

5 L. X. Zhu, F. Y. Liu, H. T. Lin, J. J. Hu, Z. F. Yu, X. R. Wang and S. H. Fan, *Light: Sci. Appl.*, 2016, **5**, e16052.

6 H. Zheng, X. B. Li, N. K. Chen, S. Y. Xie, W. Q. Tian, Y. P. Chen, H. Xia, S. B. Zhang and H. B. Sun, *Phys. Rev. B: Condens. Matter Mater. Phys.*, 2015, **92**, 115307.

7 Z. B. Zheng, J. T. Li, T. Ma, H. L. Fang, W. C. Ren, J. Chen, J. C. She, Y. Zhang, F. Liu, H. J. Chen, S. Z. Deng and N. S. Xu, *Light: Sci. Appl.*, 2017, **6**, e17057.

8 B. Radisavljevic, A. Radenovic, J. Brivio, V. Giacometti and A. Kis, *Nat. Nanotechnol.*, 2011, **6**, 147.

9 M. Zhao, Z. Ye, R. Suzuki, Y. Ye, H. Zhu, J. Xiao, Y. Wang, Y. Iwasa and X. Zhang, *Light: Sci. Appl.*, 2016, **5**, e16131.

10 J. Yang, Z. Wang, F. Wang, R. J. Xu, J. Tao, S. Zhang, Q. H. Qin, B. Luther-Davies, C. Jagadish, Z. F. Yu and Y. R. Lu, *Light: Sci. Appl.*, 2016, **5**, e16046.

11 T. F. Yan, X. F. Qiao, X. N. Liu, P. H. Tan and X. H. Zhang, *Appl. Phys. Lett.*, 2014, **105**, 101901.

12 D. A. Bandurin, A. V. Tyurnina, G. L. Yu, A. Mishchenko, V. Zólyomi, S. V. Morozov, R. K. Kumar, R. V. Gorbachev, Z. R. Kudrynskyi, S. Pezzini, Z. D. Kovalyuk, U. Zeitler, K. S. Novoselov, A. Patanè, L. Eaves, I. V. Grigorieva, V. I. Fal'ko, A. K. Geim and Y. Cao, *Nat. Nanotechnol.*, 2016, **12**, 223.

13 D. Wang, X. B. Li and H. B. Sun, *Nanoscale*, 2017, **9**, 11619.

14 D. Wang, X. B. Li, D. Han, W. Q. Tian and H. B. Sun, *Nano Today*, 2017, **16**, 30.

15 L. Z. Kou, A. J. Du, Y. D. Ma, T. Liao and C. F. Chen, *Phys. Chem. Chem. Phys.*, 2017, **19**, 22502.

16 S. Lei, L. Ge, S. Najmaei, A. George, R. Kappera, J. Lou, M. Chhowalla, H. Yamaguchi, G. Gupta, R. Vajtai, A. D. Mohite and P. M. Ajayan, *ACS Nano*, 2014, **8**, 1263.

17 S. D. Lei, X. F. Wang, B. Li, J. H. Kang, Y. M. He, A. George, L. H. Ge, Y. J. Gong, P. Dong, Z. H. Jin, G. Brunetto, W. B. Chen, Z. T. Lin, R. Baines, D. S. Galvão, J. Lou, E. Barrera, K. Banerjee, R. Vajtai and P. Ajayan, *Nat. Nanotechnol.*, 2016, **11**, 465.

18 W. Feng, W. Zheng, W. Cao and P. A. Hu, *Adv. Mater.*, 2014, **26**, 6587.

19 S. R. Tamalampudi, Y. Y. Lu, U. R. Kumar, R. Sankar, C. D. Liao, B. K. Moorthy, C. H. Cheng, F. C. Chou and Y. T. Chen, *Nano Lett.*, 2014, **14**, 2800.

20 G. W. Nudd, S. A. Svatek, L. Hague, O. Makarovsky, Z. R. Kudrynskyi, C. J. Mellor, P. H. Beton, L. Eaves, K. S. Novoselov, Z. D. Kovalyuk, E. E. Vdovin, A. J. Marsden, N. R. Wilson and A. Patanè, *Adv. Mater.*, 2015, **27**, 3760.

21 D. W. Ma, W. W. Ju, Y. N. Tang and Y. Chen, *Appl. Surf. Sci.*, 2017, **426**, 244.

22 Y. Q. Cai, G. Zhang and Y. W. Zhang, *J. Phys. Chem. C*, 2017, **121**, 10182.

23 J. Camassel, P. Merle, H. Mathieu and A. Chevy, *Phys. Rev. B: Condens. Matter Mater. Phys.*, 1978, **17**, 4718.

24 J. F. Sánchez-Royo, G. M. Matutano, M. B. Gisbert, J. P. M. Pastor, A. Segura, A. Cantarero, R. Mata, J. C. Ferrer, G. Tobias, E. Canadell, J. M. Hueso and B. D. Gerardot, *Nano Res.*, 2014, **7**, 1556.

This journal is © the Owner Societies 2018

Phys. Chem. Chem. Phys., 2018, **20**, 6945–6950 | 6949

25 V. Zolyomi, N. D. Drummond and V. I. Fal'ko, *Phys. Rev. B: Condens. Matter Mater. Phys.*, 2014, **89**, 1.

26 G. W. Nudd, S. A. Svatek, T. Ren, A. Patanè, O. Makarovsky, L. Eaves, P. H. Beton, Z. D. Kovalyuk, G. V. Lashkarev, Z. R. Kudrynskyi and A. I. Dmitriev, *Adv. Mater.*, 2013, **25**, 5714.

27 J. Gao, G. Zhang and Y.-W. Zhang, *J. Am. Chem. Soc.*, 2016, **138**, 4763.

28 Q. Chen, H. Hu, X. J. Chen and J. L. Wang, *Appl. Phys. Lett.*, 2011, **98**, 053102.

29 B. Ghosh, S. Nahas, S. Bhowmick and A. Agarwal, *Phys. Rev. B: Condens. Matter Mater. Phys.*, 2015, **91**, 115433.

30 J. S. Qi, X. Li, X. F. Qian and J. Feng, *Appl. Phys. Lett.*, 2013, **102**, 173112.

31 A. Ramasubramaniam, D. Naveh and E. Towe, *Phys. Rev. B: Condens. Matter Mater. Phys.*, 2011, **84**, 205325.

32 J. Zhou, Q. Wang, Q. Sun, P. Jena and X. S. Chen, *PNAS*, 2010, **7**, 2801.

33 A. K. A. Lu, M. Houssa, I. P. Radu and G. Pourtois, *ACS Appl. Mater. Interfaces*, 2017, **9**, 7725.

34 L. Huang, N. J. Huo, Y. Li, H. Chen, J. H. Yang, Z. M. Wei, J. B. Li and S. S. Li, *J. Phys. Chem. Lett.*, 2015, **6**, 2483.

35 L. Debbichi, O. Eriksson and S. Lebègue, *J. Phys. Chem. Lett.*, 2015, **6**, 3098.

36 P. Hohenberg and W. Kohn, *Phys. Rev.*, 1964, **136**, B864.

37 P. E. Blöchl, *Phys. Rev. B: Condens. Matter Mater. Phys.*, 1994, **50**, 17953.

38 G. Kresse and J. Furthmüller, *Phys. Rev. B: Condens. Matter Mater. Phys.*, 1996, **54**, 11169.

39 J. P. Perdew and W. Yue, *Phys. Rev. B: Condens. Matter Mater. Phys.*, 1986, **33**, 8800.

40 S. Grimme, *J. Comput. Chem.*, 2006, **27**, 1787.

41 H. H. Gürel, V. O. Özçelik and S. Ciraci, *J. Phys.: Condens. Matter*, 2013, **25**, 305007.

42 D. Wang, D. Han, X. B. Li, S. Y. Xie, N. K. Chen, W. Q. Tian, D. West, H. B. Sun and S. B. Zhang, *Phys. Rev. Lett.*, 2015, **114**, 196801.

43 A. V. Kolobov, P. Fons, J. Tominagam and S. R. Ovshinsky, *Phys. Rev. B: Condens. Matter Mater. Phys.*, 2013, **87**, 165206.

44 G. W. Mudd, M. R. Molas, X. Chen, V. Zólyomi, K. Nogajewski, Z. R. Kudrynskyi, Z. D. Kovalyuk, G. Yusa, O. Makarovsky, L. Eaves, M. Potemski, V. I. Fal'ko and A. Patanè, *Sci. Rep.*, 2016, **6**, 39619.

45 A. Politano, G. Chiarello, R. Samnakay, G. Liu, B. Gürbulak, S. Duman, A. Balandin and D. W. Boukhvalov, *Nanoscale*, 2016, **8**, 8474.

46 J. Robertson, *J. Phys. C: Solid State Phys.*, 1979, **12**, 4777.